Published in final edited form as:
J Am Chem Soc. 2013 December 4; 135(48): 18096–18107. doi:10.1021/ja406648n.

De novo designed metallopeptides with type 2 copper centers: modulation of reduction potentials and nitrite reductase activities

Fangting Yu, **James E. Penner-Hahn**, and **Vincent L. Pecoraro***

Abstract

Enzymatic reactions involving redox processes are highly sensitive to the local electrostatic environment. Despite considerable effort, the complex interactions between different influential factors in native proteins impede progress towards complete understanding of the structure-function relationship. Of particular interest is the type 2 copper center $Cu(His)_3$, which may act as an electron transfer center in peptidylglycine α-hydroxylating monooxygenase (PHM) or a catalytic center in copper nitrite reductase (CuNiR). A *de novo* design strategy is used to probe the effect of modifying charged amino acid residues around, but not directly bound to, a $Cu(His)_3$ center embedded in three-stranded coiled coils (**TRI-H**)$_3$ [**TRI-H** = Ac-G WKALEEK LKALEEK LKALEEK **H**KALEEK G-NH_2]. Specifically, the peptide **TRI-EH** [**TRI-EH** = **TRI-H**K22E] alters an important lysine to glutamate just above the copper binding center. With a series of **TRI-EH** peptides mutated below the metal center, we use a variety of spectroscopies (EPR, UV-Vis, XAS) to show a direct impact on the protonation equilibria, copper binding affinities, reduction potentials and nitrite reductase activities of these copper-peptide complexes. The potentials at a specific pH vary by 100 mV and nitrite reductase activity ranges over a factor of four in rates. We also observe that affinities, potentials and catalytic activities are strongly influenced by pH conditions (pH 5.8 ~ 7.4). In general, Cu(II) affinities for the peptides are diminished at low pH values. The interplay between these factors can lead to a 200 mV shift in reduction potentials across these peptides, which is determined by the pH-dependent affinities of copper in both oxidation states. This study illustrates the strength of *de novo* protein design in elucidating the influence of ionizable residues on a particular redox system, an important step towards understanding the factors that govern the properties of this metalloenzyme with a goal of eventually improving the catalytic activity.

Introduction

Redox-active enzymes are critical in many biological processes, with metal cofactors accounting for many of the redox-related reactions in native proteins. These activities include catalyzing important biological processes, such as photosynthesis (electron transfer and water oxidation), respiration, molecular oxygen reduction, nitrogen fixation and denitrification.[1–5] Specifically, redox-active copper sites exist in a large number of metalloproteins, which, along with iron proteins, play important roles in electron transfer, activation and transport of dioxygen and the metabolism of other small molecules.[6–16] Within the metallobiosphere, copper proteins are extremely important with functions ranging from pure electron transfer to multi-electron redox catalysis. Type 2 copper centers

*Corresponding author: vlpec@umich.edu.
Present address: Department of Chemistry, 930 N. University Ave., University of Michigan, Ann Arbor, MI 48109 1055

Supporting Information Available Detailed data fitting process, calculation, additional characterizations and Pymol models. This information is available free of charge via the Internet at http://pubs.acs.org

comprise a broad class of mononuclear sites that again serve both catalytic and redox functions. Two specific enzymes are of interest to us as they contain $Cu(His)_3$ structures. The first, peptidylglycine α-hydroxylating monooxygenase (PHM) has a $Cu(His)_3$ center (Cu_H) whose role is to donate an electron to the catalytic Cu_M site which activates dioxygen.[17–20] The second, copper nitrite reductase (NiR), is an essential component of dissimilatory nitrite reduction using a type 1 Cu center to donate an electron to the $Cu(His)_3$ active site which along with protons converts NO_2^- to NO and H_2O.[7,21–25] Thus, a structurally related $Cu(His)_3$ site can be differentially utilized based on the surrounding protein environment.

Understanding the relationship between structure and function has always been a major goal of biomimetic studies. For redox-active metalloproteins, it is obvious that the ligands coordinated to the metal center directly influence the redox properties.[26,27] However, electrostatic interactions of the redox center with the surrounding charged groups are now recognized to influence redox property modulation. Charged amino acid residues, e.g. glutamate (Glu), lysine (Lys), both in the interior and on the surface of the proteins, can participate in fine-tuning the potentials of redox-active metal sites.[28–31] Furthermore, enzymatic reactions can be highly sensitive to the local electrostatic environment. Considerable effort has been devoted to understanding the electrostatic interactions in native proteins, however, due to the complexity of native systems, it is always challenging to disentangle the contribution of each potentially influential factor.

A *de novo* design strategy provides an opportunity to generate biologically relevant models to understand structure-function relationships using a minimal construct.[32–35] With a simplified polypeptide sequence, the local environment of metal centers may be modified rationally in order to investigate the important factors that govern the properties and functions of a specific site. Previously, we reported a functional copper nitrite reductase model embedded in a *de novo* designed three-stranded coiled coil (3SCC) scaffold, which represents one of the most efficient model systems for NiR in aqueous solutions.[36] Prior to this work, there were a few cases of $Cu(His)_3$ sites in *de novo* designed peptides with controlled copper coordination.[37–39] Although redox processes have been demonstrated in a few systems,[40,41] none were fully characterized in both oxidation states. Our system was the first to have both relatively well-characterized, stable Cu(I) and Cu(II) oxidation states that exhibits NiR activity in aqueous conditions. We observed very positive reduction potentials for these systems, which probably reflected the stabilization of the Cu(I) state in a trigonal planar geometry.[36] Initial designs focused solely on the first coordination sphere of copper, yielding modest catalysts. To design a model with higher rates the next logical step is to explore systematically secondary coordination sphere modifications around the copper. Of course, such studies are potentially relevant to understanding how solely electron transfer centers as found in PHM are influenced by the same secondary coordination sphere modifications. We report herein, a series of peptides (Table 1) modified based on the parent peptide **TRI**L2WL23H (**TRI-H**), which address how the local environment, particularly charged residues, influence the redox properties and catalytic behaviors of these designed copper proteins. The models for Cu(I)(**TRI-H**)$_3$ and the other peptides used are given as Figure 1.

Experimental methods

The sequences of the peptides used in this work are shown in Table 1 with each heptad repeat given as *abcdefg*. Variations were made at the *b*, *e*, *g* positions of the heptad in addition to the L23H mutation.

General procedures

The copper-peptide complexes were prepared by adding a solution of Cu(I) tetra(acetonitrile) tetrafluoroborate or Cu(II) chloride into a (buffered) solution of apo-peptide. Since the Cu(I)-peptide complexes undergo slow oxidation under aerobic conditions, all reactions concerning Cu(I) or nitrite reduction were carried out in an inert atmosphere box.

Peptide synthesis and purification

All peptides in this work were synthesized on an Applied Biosystem 433A peptide synthesizer using standard protocols[43] and purified and characterized as previously reported[44]. The apo-peptide solution was prepared by dissolving purified dry peptides in doubly distilled water or buffer solutions. The peptide concentration was determined based on the tryptophan (Trp) absorbance at 280 nm (ε = 5500 $M^{-1}cm^{-1}$).[45]

Ultraviolet-Visible (UV-Vis) and fluorescence spectroscopy

UV-Visible spectra were collected in quartz air-tight cuvettes at 25 °C on a Cary100 Bio UV-Vis spectrophotometer. Emission spectra were recorded on a Fluomax-2 Fluorimeter at 25 °C.

pK_a determination for Cu(II)-peptides

The deprotonation of Cu(II)-peptides was reflected on the UV-Visible spectra. The UV-Visible spectra of a solution containing 0.27 mM Cu-3SCC and 0.03 mM apo-3SCC (to ensure that > 99 % of Cu(II) is bound to the peptide) at various pH conditions were collected and pK_a fitted to equation (1). Assuming the protonation equilibrium corresponds to *n* protons, this can be described as following:

$$EH_nK_a \rightleftharpoons nH^+ + E^{n-} \quad \text{equation (1)}$$

The total molar extinction coefficient at a particular wavelength can be written as:

$$\varepsilon_{total} = \frac{\varepsilon_E + \varepsilon_{EH_n} \bullet 10^{n(pK_a - pH)}}{1 + 10^{n(pK_a - pH)}}$$

where ε_E and ε_{EH_n} stand for the extinction coefficients of individual species in different protonation states.

Binding constants determination

Cu(I) binding constants—The affinity of peptide trimers (pep_3) to Cu(I) was determined by competitive binding assay with disodium bathocuproindisulfonate (Na_2BCS, BCS) or disodium bacinchoninate (Na_2BCA, BCA) as a competitive chelator in 50 mM potassium phosphate buffer. The competition equilibrium for the titration experiment can be expressed by the following chemical equation:

$$Cu\text{-}pep_3 + 2L\ (BCS \text{ or } BCA) \rightleftharpoons CuL_2 + pep_3$$

Starting with 40 μM of Cu(I)-pep_3, 40 μM apo-pep_3, small aliquots of a 5.00 mM BCS or BCA stock solution were added into the system. Transfer of Cu(I) from Cu-pep_3 to CuL_2 was tracked from the absorbance at 483 nm for L = BCS (ε = 13,000 $M^{-1}cm^{-1}$) and at 562 nm for L = BCA (ε = 7,900 $M^{-1}cm^{-1}$).[46–48] Titrations were carried out in triplicates and the

dissociation constants were fitted by spectrophotometric and/or potentiometric data fitting program Hyperquad 2006, taking the reported dissociation constants for $Cu(I)L_2$.[46–48] At both pH 7.4 and pH 5.8, titrations were performed to investigate how the affinities change in relation to pH. At pH 5.8, the concentration of the protonated form of the ligand BCS was taken into account.[47,48]

Cu(II) binding constants—As reported previously, the Trp emission at 350 nm decreases upon Cu(II) binding to the $(His)_3$ pocket.[36] A stock solution of $CuCl_2$ was added to ~800 nM 3SCC in 50 mM buffer solution. Triplicate titrations were carried out and data fitted with Hyperquad 2006.

X-Ray absorption spectroscopy (XAS)

A 1 mM Cu(I)(**TRI-EH**)$_3$ solution was prepared by adding 0.8 eq. (*wrt*. peptide trimer) Cu(I) tetra(acetonitrile) tetrafluoroborate solution to the peptide buffer solution in an inert atmosphere box. The pH of the solution was adjusted to 8.5 using small aliquots of concentrated KOH. Glycerol was added as a glassing agent. The homogeneous mixture of 50% aq. 50% glycerol solution was then transferred to a sample cell and frozen at liquid nitrogen temperature. Data were collected at Stanford Synchrotron Radiation Lightsource (SSRL) on beamline 7–3 with a Si(220) double-crystal monochromator, a flat Rh-coated harmonic rejection mirror and a 30-element Ge array detector. An Oxford Instruments liquid helium cryostat was used to keep the samples below 10 K during data collection. Data were collected as fluorescence excitation spectra and normalized to the incident intensity measured with an N_2-filled ion chamber. Data were measured with steps of 0.25 eV in the XANES region (1 s integration time) and $k = 0.05$ Å^{-1} to 13.5 Å^{-1} in the EXAFS region (1–20 s integration, k^3 weighted). Energies were calibrated by assigning the lowest energy inflection point of a copper metal foil as 8980.3 eV. An initial E_0 value of 9000 eV was used to convert data to *k*-space, and the background was removed using a three-region cubic spline. EXAFS data were analyzed using EXAFSPAK[49] with *ab initio* amplitude and phase parameters calculated using FEFF 9.0[50]. Imidazole outer-shell scattering was modeled using phase and amplitude parameters calculated for an idealized $Cu(imid)_4$ structure, with Debye-Waller factors defined as suggested by Dimakis and Bunker[51]; the imidazole was refined as a rigid group with distances and Debye-Waller factors linked to the refined Cu-N parameters such that there were only 3 variable parameters (R_{Cu-N}, σ^2_{Cu-N}, and ΔE_0).

EPR spectroscopy

X-band EPR spectra were collected on a Bruker EMX electron spin resonance spectrometer with a Varian liquid nitrogen cryostat at 77 K. A sample of ~1mM Cu(II)$(3SCC)_3$ was prepared in a 50 mM buffer solution, and the pH was adjusted by adding concentrated HCl or KOH solution into the sample. An extra 0.5 mM apo-3SCC was added to ensure that the free Cu(II) is less than 0.1 %. 50% glycerol was used as a glassing agent. The EPR parameters were extracted by fitting the collected spectra to the simulated spectra using the EPR data fitting software SpinCount.

NiR activity reaction rates

The rates were determined as previously reported for Cu(**TRI-H**)$_3$.[36] 30 mM $NaNO_2$ was mixed with 0.18 mM Cu(II)(3SCC) and 0.09 mM apo-3SCC (to ensure that over 99% of Cu(II) is bound to the peptide). The reaction was initiated by adding 6 equivalents of sodium ascorbate (NaAsc) with respect to Cu(II). The consumption of sodium ascorbate (NaAsc) was monitored by UV-Visible spectroscopy. The control was a mixture of 30 mM $NaNO_2$ and 0.09 mM apo-3SCC with the same amount of NaAsc. The rates of the reaction were calculated by two times the different rates of NaAsc consumption (decrease of absorbance at

251 nm) between the sample and the control. The production of nitric oxide was examined using the method previously reported.[36]

Results

pK_a of Cu(II)-peptides

For the parent peptide **TRI-H**, the appearance of a broad band with a maximum absorbance at 644 nm (Figure 2A) was observed as the pH of a Cu(II)(**TRI-H**)$_3$ was increased from 2.92 to 5.52. This spectrum has previously been suggested to be Cu(II)(His)$_3$ $(OH_2)_{1–2}$.[36] When the pH was raised above 7.6, a new set of spectra was observed which contained an isosbestic point at 571 nm (Figure 2B). The absorbance at 644 nm decreased while a new band at 514 nm grew in intensity. By fitting the absorbance at 644 nm to equation (1), a pK_a value corresponding to the changes in the absorption spectra described above was extracted (Table 2), which corresponds to a one-proton deprotonation process.

Interestingly, the pH titration of Cu(II)(**TRI-EH**)$_3$ resulted in a pK_a distinctively different from the parent peptide (Table 2). Again, from the pH region 2.97–5.57, the increase of absorbance at 659 nm is indicative of copper binding to the peptide and is reminiscent of the parent peptide (Figure S1). However, when the pH was raised from 5.33 to 7.87, the absorbance at 659 nm decreased slightly (Figure 3), resulting in a pK_a = 6.33. This deprotonation event fitted best to a 1.65(23) proton process (Figure S1B), which suggested that the nature of this deprotonation might be different from the one for Cu(II)(**TRI-H**)$_3$. Similar effects were also observed for Cu(II)(**TRI-EH**K24E)$_3$ (Figure S2). The Cu(II) d-d band evolves differently upon pH increase for different peptides within the pH region that we are interested in. (Figure 4) In summary, we observed the appearance of Cu(II) d-d band when bound to different peptides and the transformations of the spectra are pH-dependent due to various deprotonation events.

Cu(I) and Cu(II) affinities, the free energy of binding and calculated reduction potentials

Dissociation constants for the complexation of either Cu(I) or Cu(II) at pH 5.8 and 7.4 for each of the peptides studied in this work are provided in Table 3. The first point to recognize is that the reversal of the position of the Lys and Glu groups going from **TRI-H** to **TRI-EH**E27K leads to a marked change in the Cu(I) affinity (a factor of 100 in favor of the reversed peptide), while the corresponding Cu(II) affinities are higher for the original parent peptide. In an effort to isolate the effects, peptides solely with modifications at the 22 position, which is much closer to the copper site than the 27 position (Figure 1) were examined. At pH 7.4, for the series **TRI-EH**, **TRI-H**K22Q and **TRI-H** corresponding to Δ_{charge} = −6, −3 and 0, respectively, the Cu(I) affinity changed only modestly (a factor of 5 less stable for **TRI-H**K22Q and essentially identical for **TRI-EH**) and the Cu(II) affinities were essentially invariant. At pH 5.8, the mutated peptides **TRI-H**K22Q, **TRI-EH** have very similar affinities and reduction potentials (Table 4), although they have higher Cu(I) affinities and lower Cu(II) affinities compared to the parent peptide **TRI-H**. It is worth noticing that **TRI-H** behaves quite differently compared to the mutated peptides at pH 5.8, possibility due to the lower pK_a that the mutated peptides have; however, it appears that Δ_{charge} of the residues at the 22nd position (one residue above the binding site His23) does not have a dramatic influence on the affinities and redox properties of the peptide. Based on these observations, we chose to examine a series of peptide substitutions that occur below the copper-binding site (positions 24 and 27) using the K22E derived peptides as this would allow for the widest range in Δ_{charge} (from 0 to −12).

As shown in Figure 5A, the Cu(I) affinities for the series of peptides containing a K22E substitution are related to the total charge around the copper binding site at both pH 5.8 and

7.4. As the total negative charge is increased, going from $\Delta_{charge} = 0$ (**TRI-EH**E27K) to $\Delta_{charge} = -12$ (**TRI-EH**K24E), the Cu(I) affinity decreased by about two orders of magnitude, which occurred under both pH conditions. However, the Cu(II) affinities seemed to be relatively immune to the change of total charge. As shown in Figure 5B, at both pH 5.8 and pH 7.4, the change of Cu(II) affinities to the peptides was minimal at a particular pH across the series of peptides with different total charge. It is interesting to notice that unlike Cu(I), whose affinities remained essentially the same for a particular peptide at different pH conditions with dissociation constants ranging from picomolar to femtomolar, Cu(II) was destabilized by at least two orders of magnitude when the pH decreased from 7.4 to 5.8, as shown in Figure 5B. The difference between Cu(I) and Cu(II) can be described more clearly when we compare the free energy of binding (Supporting Information 4) at a particular pH. (Figure 6)

While reduction potentials for metalloproteins and small molecules are often determined by direct electrochemical methods, one may extract the same information by determining the binding affinities of the metals in both oxidation states to the proteins and applying the Nernst Equation. This approach has the added benefit that it allows one to track directly the behavior of interest (*e.g.*, reaction rates) not only against the reduction potential, but also to see if correlations exist associated with a specific oxidation level. The reduction potentials of the Cu(II)/Cu(I)-peptide system were calculated using the methodology shown in Scheme 1 and equation (2), where $E°_{(Cu, aq)} = 0.159$ V *vs*. NHE was utilized (Table 4).[36,52] Since the free energy of binding for Cu(I) varies with amino acid substitution more than that of Cu(II) (Figure 6), the change in the calculated reduction potential is dominated by the variation of Cu(I) affinities. This is true at both pH conditions; however, the change in potential between pH conditions is due to the stabilization of the Cu(II) upon acidification. The linear regressions for the trends following amino acid substitutions resulted in two parallel lines, the distance between which was about 100 mV. This value corresponds to a 1 H^+ per electron change in potential which is consistent with the difference of 1.6 pH units for these measurements. (Figure 7)

$$E^{o}_{(Cu(pep)_3)} = E^{o}_{(Cu,aq)} - \frac{2.303RT}{nF}\log\frac{K_{d(Cu(I)(pep)_3)}}{K_{d(Cu(II)(pep)_3)}} \quad \text{equation (2)}$$

XAS of Cu(I)(TRI-EH)$_3$

The XANES spectra of Cu(I)(**TRI-EH**)$_3$ and Cu(I)(**TRI-H**)$_3$ (Figure 8A) both show a modest intensity peak at ~8983 eV; this is typical of Cu(I) in an approximately trigonal environment.[53] The near identity of these spectra shows that there are only minor structural differences between the copper sites. The EXAFS data for Cu(I)(**TRI-EH**)$_3$ (Figure 8B, C) support this structural interpretation. The Fourier transform is dominated by a peak at R + a $\approx$ 1.5 Å typical of Cu-N or Cu-O nearest neighbor scattering, with pronounced outer-shell scattering typical of rigid ligands such as histidine. Quantitative fitting (Table 5) confirms this structure. The nearest-neighbor distance of 1.93 Å is typical of three-coordinate Cu(I), and the outer-shell scattering can be modeled using three imidazole ligands, results that are quantitatively consistent with structural parameters reported previously for Cu(I)(**TRI-H**)$_3$.[36] Attempts to fit the data with a Cu-O shell in addition to, or in place of one of the Cu-imidazole interactions did not give any improvement in the fit. (Table S6)

EPR analyses of Cu(II) peptides

The EPR spectra of Cu(II)(**TRI-H**)$_3$ were collected from pH 5.87 to pH 9.14, which showed a transition of A_{II} and g_{II} from pH 7.80 to pH 9.14 (Supporting Information 3). The EPR

parameters of Cu(II)(**TRI-EH**E27K)$_3$, Cu(II)(**TRI-EH**)$_3$ and Cu(II)(**TRI-EH**K24E)$_3$ at both pH 5.8 and 7.4 were in the same range as the parent peptide complex (Table 6). Specifically, the $g_{\perp}$ is smaller than the g_{II} and the A_{II} of all these complexes are in the range of 17 – 19 mT, indicative of a type 2 copper center with a high coordination number (4 or 5), which is consistent with the observed d-d bands in the UV-Vis spectra.

NiR activity

The Cu-peptides exhibit NiR activity with different rates (Figure 9), all of which are pH dependent. Specifically, as the total negative charge was increased from 0 to −12, the rates of the reaction increased by about four fold. Moreover, the rates are also correlated to the calculated reduction potential at pH 5.8, as shown in Figure 10: as the calculated reduction potentials increase, the rates decrease. The turnover numbers (TONs) for these reactions, expressed as mole of electrons per mole of copper, were obtained. The TONs in one hour are linearly associated with the local negative charge (Figure S6). As we increased the Δ_{charge} from 0 (**TRI-EH**E27K) to −12 (**TRI-EH**K24E), the TONs at pH 5.8 increased by one. For all of the NiR reactions, we did not observe any degradation of the enzyme 1.5 h after the reaction was initiated. Nitric oxide production was confirmed for the peptides showing the slowest and fastest rates [Cu(**TRI-EH**E27K)$_3$ and Cu(**TRI-EH**K24E)$_3$, respectively] at pH 5.8. (Supporting Information 8)

Discussion

The environment that surrounds redox sites plays a critical role in determining the redox potentials and pathways for electron flow in proteins, however, in most cases, multiple factors exert influence on the redox potential simultaneously, complicating the understanding of the structure-function relationship of a particular system. Conceptually, we can think of the energy associated with the redox process as the sum of the inner-sphere contributions, which directly point to the energy needed to add or remove an electron to the redox site, and outer-sphere contributions, which are related to the interaction of the redox site with the protein and solvent environment during the redox process.[54] In reality, more often than not, one change around the active site may lead to a cascade of events that will eventually modify the redox properties, but it is challenging to track down the specific roles of each event.

A significant amount of work has been done to understand the redox property modulations on systems containing heme cofactors or cupredoxin sites. It was reported, as early as 1989, that mutating the valine (Val) residue into charged or polar residues such as Glu, aspartate (Asp) and asparagine (Asn) led to a decrease in the mid-point redox potential of recombinant myoglobin at 25 °C, which demonstrated that changing the electric field around the redox center resulted in a substantial change in the redox thermodynamics of a particular system.[30] Specifically, the substitution of Val68 close to the distal site of the heme center into a Glu or an Asp led to about 200 mV decrease in the reduction potential whereas Val68Asn resulted in an 80 mV decrease. Furthermore, the Dutton and Gibney groups showed that by varying the burial of heme in the hydrophobic core, heme peripheral substituents, heme-hydrophobic amino acids, *et al*., they were able to modulate rationally the heme-protein redox potential over a range of a few hundred mV.[55–58] More recently, Yi Lu and coworkers demonstrated that the redox potential of a cupredoxin site in azurin could be tuned by modifying two important secondary coordination sphere interactions: hydrophobicity and H-bonding. Their work demonstrated an astounding shift in redox potentials, in some cases by as much as 700 mV, which extended even beyond the natural redox potential range of the protein.[59,60] To our current knowledge, there are no systematic

studies on the redox property modulations of $Cu(His)_3$ site in a protein environment, despite its importance in the electron transfer or catalytic functions in native proteins.

Taking advantage of a *de novo* protein design approach, we took a known functional peptide $Cu(\mathbf{TRI\text{-}H})_3$, and then modified the local charge in a stepwise manner in order to observe changes in the reduction potentials and NiR activity of a series of peptides (Table 1). The rationale of the design was first to invert the charged residues Glu27 and Lys22, yielding **TRI-EH**E27K. Compared to the parent peptide **TRI-H**, the change in the overall charge, or Δ_{charge}, of this peptide is 0. While this double mutation led to a significant shift in potential, we observed that there was no perturbation in the reduction potentials between copper complexes of **TRI-H** and **TRI-EH** at pH 7.4. We used the K22E mutation (**TRI-EH** scaffold) to evaluate a broader ranger of charge effects than would be available with **TRI-H**. We substituted the residues of **TRI-EH** in a stepwise manner below the $Cu(His)_3$ site from positively-charged residues into neutral and then negatively-charged residues. Since we have three strands of peptides self-assembling in aqueous solutions above pH 5,[61] the resulting series of peptides have a Δ_{charge} of −0, −3, −6, −9 and −12. None of the residues (Lys22, Lys24 and Glu27 in **TRI-H**) involved in the mutations are inside the helix bundle, neither can they directly coordinate to the copper center (according to our pymol models shown in Figure 1), hence we do not expect to see first coordination sphere effects on the properties of the copper center. This *de novo* design strategy allows us to vary the charge systematically in order to probe the subtle influence of surface charged residues on the stability constants of Cu(I) and Cu(II) protein forms and, subsequently, upon the redox properties and catalytic activities of these type 2 copper centers.

We first characterized the binding of the Cu(II) ion to the peptide as a function of pH using UV-Vis spectroscopy as is shown in Figures 2–4. Before considering these spectra, it is worth recognizing that there are multiple pH-dependent reactions that can occur between pH 2.5 and 8.0 that can affect the chemistry in the system. First, the conversion of two-stranded coiled coils (2SCCs) to 3SCCs is known to occur upon the deprotonation of Glu at *e* positions with a pK_a~4.0–4.5.[35,62] This behavior has been noted for several peptides of the **TRI** family, but most notably for **TRI-H**.[36] Second, the copper binding ligand can undergo deprotonation of the cationic imidazolium form, which does not bind copper, to the neutral imidazole, which binds to copper.[63] A ^{1}H NMR titration of $(\mathbf{TRI\text{-}H})_3$ has shown that this deprotonation event occurs over the pH range 5.5–8.0 in the absence of metal.[36] Most likely, the presence of a Lewis Acid shifts the imidazolium to imidazole equilibrium in favor of the neutral metal binding ligand as has been reported for both Zn and Cu complexes with $(\mathbf{TRI\text{-}H})_3$.[36,42] Furthermore, under higher pH conditions the imidazole may be converted to the negatively charged imidazolate form, which also binds to copper efficiently. It is generally believed, however, that this equilibrium occurs at much higher pH values than investigated here. Additional carboxylic acid deprotonation events would be expected when Lys is substituted to Glu at the 22 and/or 24 positions for the mutated peptides. One would expect this deprotonation chemistry to occur in the general range of the pre-existing carboxylic acids at the *e* positions of the peptide. At very high pH conditions (again above pH 8), the deprotonation of the Lys side chain may become relevant, which could disrupt the 3SCCs; however, the conditions used in this study are unlikely to enter this basic range. Finally, when copper is bound, and if a water is bound to the copper, the deprotonation of Cu(II)-bound water could occur in the basic pH region.

An examination of the pH dependent trends in Figure 4 demonstrates that **TRI-H**, **TRI-EH**E27K, **TRI-EH**, and **TRI-EH**K24E all exhibit a sharp rise in absorbance moving from pH 3 until the spectra level out by ~pH 5. Two major processes are occurring over this pH range. The first is the conversion of the 2SCCs to 3SCCs through deprotonation of Glu. This conversion for the apo-peptide is not reflected in these spectroscopic changes. The second

process is the binding of the Cu(II) to the 3SCCs which is directly reflected by these spectra as they arise from the d-d transition of Cu(II). Previous analysis of this copper site for Cu(II)(**TRI-H**)$_3$ using EPR spectroscopy suggested that this system is probably a five-coordinate Cu(II) with three coordinated imidazoles and two solvent molecules.[36] The UV-Vis spectra of all these peptides are consistent with the same chromophore until at least pH 6.0. As the pH is raised to neutral conditions, peptides containing additional Glu (**TRI-EH**, and **TRI-EH**K24E) show an additional pH-dependent conversion (pK_a~6.5). This process could be due to A) the deprotonation of the copper coordinated water, B) complexation of Glu22 to the copper, or C) the deprotonation of Glu22 leads to the formation of an H-bond either with a coordinated His or to a bound water. We disfavor the explanations that Glu22 binds directly to Cu(II) or forms a hydrogen bond with coordinated water as the orientation of the Glu on the helix places it too far from the metal center to interact in these ways. This observation leaves the most likely explanations for the pK_a in the 6–7 range for peptides containing the K22E mutations as metal bound water deprotonation or the deprotonation of the glutamic acid leading to the H-bond formation between Glu22 and His23.

As shown in Figure 2B, Cu(II)(**TRI-H**)$_3$, which does not contain the K22E modification, exhibits a second significant absorption change at a higher pH value with a pK_a of 8.53. This is thought to be associated with the deprotonation of the Cu(II)-bound water into a Cu(II)-bound hydroxide because the blue shift upon this deprotonation is in accordance with the prediction of the same process in an equatorially-coordinated Cu(II) complex.[64] Spectral perturbations over this range were also observed in the EPR spectra of Cu(II)(**TRI-H**)$_3$. Going from pH 7.80 to pH 9.14, the g_{II} decreased from 2.27 to 2.26 while A_{II} increased from 18.58 to 19.29 mT (Table S2). This observed trend is consistent with the reported case of the copper-bound water deprotonation at the type 2 copper center in the mercury derivative of laccase.[65] This piece of evidence, combined with the transformation of UV-Vis spectra in this pH region, leads us to believe that the pK_a at 8.53 for Cu(II)(**TRI-H**)$_3$ corresponds to a Cu(II)-bound water deprotonation, producing a Cu(His)$_3$(OH)(OH$_2$)$_{0–1}$ species. Also consistent with the UV-Vis spectra, Cu(II)(**TRI-H**)$_3$ EPR spectra stay unchanged in the pH region 5.8 to 7.4, indicating that Cu(II) is likely to maintain a Cu(His)$_3$(OH$_2$)$_{1–2}$ coordination, with three quasi-in-plane imidazoles and one or two water molecules.[36]

In contrast, for the **TRI-EH** series of peptides, we observed different EPR parameters at pH 5.8 and 7.4. For the charge "flipped" peptide Cu(II)(**TRI-EH**E27K)$_3$, g_{II} stayed the same while A_{II} increased by 0.14 mT and the isotropic hyperfine splitting constant A_{iso} increased by 0.31 mT (Table 6). Similar changes of g_{II} and A_{iso} occurred for Cu(II)(**TRI-EH**)$_3$. For Cu(II)(**TRI-EH**K24E)$_3$, however, both g_{II} and A_{II} decreased significantly while $A_{\perp}$ increased, leading to an increased A_{iso}. In summary, the A_{iso} of the **TRI-EH** series of copper-peptide complexes increased when pH rises from 5.8 to 7.4, indicating a higher spin-density at the copper center. The changes of the other EPR parameters are dissimilar to those of Cu(II)(**TRI-H**)$_3$ in a higher pH region (7.8 to 9.1), which implies that this equilibrium (corresponding to pK_a ~6.5) is probably not a Cu(II)-bound water deprotonation.

Considering the combined observation, we assign the pK_a at ~ 6.5 for some of the **TRI-EH** peptides to a deprotonation equilibrium of a glutamate side-chain (probably at the 22 position) which can become an H-bond acceptor for the imidazole proton at the 23 position. This H-bond leads to the variance of both UV-Vis and EPR spectral parameters of the Cu(II) center. Consistent with this assignment, when the same pH titration was carried out for Cu(II)(**TRI-H**K24E)$_3$, where the Glu was placed at the 24th, instead of the 22th position, we did not observe a protonation equilibrium in this low pH range. (Figure S4, Table S1) For the charge "flipped" peptide Cu(II)(**TRI-EH**E27K)$_3$, one might have expected it to behave more similarly to the other **TRI-EH** peptides having a lower pK_a; however, models suggest

that Glu22 can interact with Lys27 in **TRI-EH**E27K which would weaken the H-bonding interaction of Glu22 with His23. This putative H-bond would lead to a less acidic Cu(II), which would increase the pK_a for the Cu(II)-bound water deprotonation in these peptides. Correspondingly, we observed a higher pK_a (9.6–9.8) for the **TRI-EH** series of peptides, which we assign as the deprotonation of the Cu(II)-bound water. (Table S1)

At pH 5.8 and 7.4, we determined the binding affinities of Cu(I) and Cu(II) to the series of peptides prepared in this work in order to evaluate the reduction potentials and the impact of protein mutations at both oxidation levels (Table 3, Figure 5 and Figure 6). These peptides were prepared in order to examine the effect of increased local negative charge on the stabilities of Cu(I) and Cu(II) within the hydrophobic core. It was thought that the Cu(II) state would be more greatly stabilized by higher negative charge, decreasing the reduction potential of the system. While the reduction potentials (Table 4) were made less positive by increasing the local negative charge, contrary to our expectation, this shift occurred as a result of Cu(I) destabilization rather than Cu(II) stabilization. These results are most clearly visualized when comparing the free energy of binding shown in Figure 6.

In contrast, Rorabacher and coworkers have reported a series of potentially tetradentate copper complexes which vary neutral nitrogen or sulfur donors over the range N_4 to NS_3. The reduction potentials of these compounds were strongly influenced by the stability constants of the Cu(II) oxidation level rather than those of the Cu(I) complexes.[66,67] In particular, an increase in the stability constants of Cu(II) complexes by as much as 10^4 ~ 10^5-fold was observed when substituting thioether sulfurs for unsaturated nitrogens; at the same time, the stability constants of Cu(I) complexes were maintained in the range 10^{14} ~ 10^{16} M^{-1}. These changes lead to differences in the reduction potentials that spanned 1.5 V.[66] The redox potentials were also observed to be pH-dependent below pH 5 (and invariant above this pH) due to the acid-base chemistry of the ligand.[68] Important differences between these models and our system include the choice of ligands (neutral thioethers and pyridyl groups), the lack of potential H-bond acceptors (such as glutamate), the lack of charge variation across the series and the possibility of a tertiary amino nitrogen atom that could serve as a fourth ligand. Hence, our system provides a more biologically relevant example to assess how electrostatic and H-bonding influence copper protein reduction potentials.

As shown in Figure 5, the relative Cu(I) or Cu(II) affinity change across the series of designed protein mutants is independent of pH as demonstrated by the invariant slopes of the lines for either oxidation state. This statement is not intended to suggest that pH is not important in this system, as marked effects are seen both on Cu(II) stability and reduction potential. As was shown, the Cu(I) stabilities are more sensitive to protein modification ($\Delta(\Delta G_a^{Cu(I)})$~ 2 Kcal/mol *versus* $\Delta(\Delta G_a^{Cu(II)})$~ 0.7 Kcal/mol, whereas one sees that the Cu(II) affinities are more sensitive to pH adjustment ($(\Delta G_a^{Cu(I)})$pH 7.4-($(\Delta G_a^{Cu(I)})$pH 5.8) ~ 0.5 Kcal/mol *versus* ($\Delta G_a^{Cu(II)}$)pH 7.4 - ($\Delta G_a^{Cu(II)}$)pH 5.8 ~ 3.5 Kcal/mol), Thus, the trend is that as the negative charge around the copper center is increased via protein modification, the Cu(I) is destabilized and the reduction potential becomes less positive. In contrast, as the pH is lowered, the Cu(II) affinity decreases and the reduction potential (Table 4) becomes more positive. Within the series there is an ~100 mV shift in potential from pH 7.4 to 5.8 for any peptide, providing a slope of ~ 60 mV/pH unit that indicates that the change in potential is dependent upon a single proton per electron. The differences between the copper affinities lead to the two parallel lines shown in Figure 7. Thus, by controlling the peptide sequence and the pH, one can systematically vary the reduction potential in this system by nearly 200 mV.

The observed trends can be explained by the change of H-bonding and salt bridge interactions around the copper center upon protein mutations under different pH conditions.

The mutation of Lys at 22 position into a Glu would likely lead to an H-bonding interaction between the carboxylic acid/carboxylate from Glu and the imidazole from His, therefore, we see pH-dependent Cu(II) affinities and reduction potentials. Variations on the other charged residues would alter the salt-bridging interactions, leading to differences in the electron-donating abilities of the imidazoles or structural changes to the Cu(I) center. Consistent with this idea, we see that **TRI-H** exhibits a modest shift to a **less** positive potential ($\Delta = -30$ mV) from pH 7.4 to 5.9 while all of the peptides with Gln or Glu in the 22 position show significant shifts to **more** positive potentials ($\Delta = +60$ to $+140$ mV) as the pH is decreased (Table 4). One possible H-bonding system that supports both the pH trends in Cu(II) binding and the impact of side chain mutations of the Cu(I) affinities is provided in Supporting Information 9.

Alteration of the peptide in the layer above the copper site (22) has virtually no effect on the reduction potential of the system (at pH 7.4: **TRI-H** $E^0 = 433$ mV; **TRI-H**K22Q $E^0 = 450$ mV; **TRI-EH** $E^0 = 440$ mV). In general, with peptides containing the K22E modification (i.e., those where mutations are made to **TRI-EH**), one observes that increasing the side chain positive charge below the metal site causes significant stabilization of the Cu(I) oxidation level, while the Cu(II) state is mildly stabilized by the same mutation. Thus, if we take **TRI-EH** as the parent peptide, replacing Lys at the 24 position with Gln and Glu progressively destabilizes Cu(I) binding, whereas converting Glu27 into Gln or Lys yields much higher Cu(I) affinities. If this were solely an electrostatic effect, one might expect the opposite trend for Cu(I) affinity (as more positive charge around the positive metal should destabilize binding) and that the greater effect would be observed for the Cu(II) level (as charge repulsion would be greater). These observations suggest an alternative explanation is required. Our best explanation is that this may again reflect H-bonding and salt bridging between the different surface residues. In the case of Cu(I)-peptides, the dominant factor may be structural perturbations that occur at the metal center.

In order to form an effective geometry for directional H-bonding and salt bridging interactions, the imidazoles may need to reorient to minimize the conformational changes on the peptide backbone, leading to a more trigonal planar or tetrahedral Cu(I) structure. Our present best explanation for the decreased Cu(I) affinity as the H-bond is formed is based on this geometric argument, rather than electronic factors. It was previously shown that Cu(I) in **TRI-H** forms a distorted trigonal planar structure.[36] We examined the parent peptide for the series of peptides reported here: **TRI-EH**, forming a direct comparison to **TRI-H**. XANES data revealed that Cu(I) coordination number did not change when we substituted a Glu in the Lys22 position, which is consistent with the fact that the affinity of Cu(I) at this pH range does not change much going from **TRI-H** to **TRI-EH**. The subtle differences of the edge structure are consistent with small changes in the symmetry of the site. For example, the small decrease in the intensity of the 8983.4 eV would be consistent with a change from a more T-shaped geometry to a more trigonal planar structure,[53] consistent with our predictions. The EXAFS fits suggest relatively large disorder in the Cu(I) site. The fitted σ^2 values for Cu(I)(**TRI-EH**)$_3$ are smaller than those found for Cu(I)(**TRI-H**)$_3$,[36] indicating that there is somewhat less variation in the Cu-N distances for Cu(I)(**TRI-EH**)$_3$. This is consistent with the suggestion, based on the XANES, that the Cu(I) site in Cu(I)(**TRI-EH**)$_3$ is somewhat more symmetric than that in Cu(I)(**TRI-H**)$_3$.

It is likely that a similar, possibly even more rigid trigonal plane exists for **TRI-EH**E27K because of the inter helical H-bonding network formed, connecting His23-Glu22-Lys27 from the adjacent strands that would hold the copper coordinating ligand His in a relatively constrained environment. (Figure S9) This is of great relevance to the rack-induced binding hypothesis proposed for blue copper electron transfer centers in native proteins.[69] This hypothesis suggests that the protein matrix is responsible for maintaining a proper metal

coordination environment and fine-tuning the redox potential to facilitate electron transfer processes. Of great interest to us is a report that demonstrates the importance of an H-bond close to the type 1 copper center in plastocyanin, which contributes to the rigidity of the coordinating environment of the type 1 copper center.[70] The higher reduction potential of Cu(**TRI-EH**E27K)$_3$, is reflective of the rigidity at the copper centers that favors a trigonal Cu(I). This can explain the difference between our system and Rorabacher's complexes mentioned earlier. In our case, the Cu(II) state is more structurally dynamic while Cu(I) is more rigid. As a result, the modulation of reduction potentials is dominated by the variance in the Cu(I) state. In Rorabacher's case, the small molecule scaffold is relatively rigid for both oxidation states, so the stability constants of the higher oxidation state are more dramatically influenced by the number and nature of the donor atoms, the chelate ring size and the general ligand topology, while little variation is observed for the lower oxidation states.

For **TRI-EH**K24E, while Glu22 forms an H-bond with His23, the charge repulsion between Glu22, Glu24 and Glu27 on the neighboring helices might force the imidazoles to adopt a tetrahedral geometry. Such perturbations in geometry are not required for the Cu(II) site as it is believed that this ion is already five-coordinate with the imidazoles no longer planar. For Cu(II), the influence of salt-bridging and H-bonding effects are not as pronounced. This point may be understood most simply. Cu(II) being much more Lewis acidic should lead to acidification of the coordinated imidazole proton. Thus, regardless of competing salt bridges, the Glu22 substitution may lead to an H-bond of sufficient stability not to be diminished significantly by salt bridging effects and protein mutations.

We next examined how side chain modifications would affect the known catalytic activities of this system. The nitrite reductase (NiR) activity of these peptides is expressed as the rates of ascorbate consumption. The influence of reduction potential on the NiR rates is clearly revealed when examining the rates at a constant pH. At pH 5.8, for the **TRI-EH** series of peptides, the higher the reduction potential, the lower the rates. (Figure 10) The reduction potential changes from 597 mV (**TRI-EH**E27K) to 491 mV (**TRI-EH**K24Q), leading to a 3.5 fold increase in the rates (from 1.07(65) × 10^{-6} M min^{-1} to 3.75(76) × 10^{-6} M min^{-1}). While there is an impressive linear correlation between rates and reduction potential, one must use caution to ascribe this effect to electron transfer since our studies show that the rapid reduction of Cu(II) to Cu(I) by ascorbate can not be rate limiting. More likely, the significant reorganization energy due to the change of coordination geometry from Cu(I) [3-coordinate] to Cu(II) [5-coordinate] limits the observed rates.

The nitrite reduction rates also increased markedly with decreasing pH, which was observed for both the parent peptide[36] and the mutated peptides (Table S4). The native CuNiR is also reported to exhibit pH-dependent activities that are proposed to be closely related to both the electron transfer process and the nitrite binding step at the catalytic site.[23] In our case, since we do not have a type 1 electron transfer site, and the reduction of the Cu(II) by ascorbate is much faster than the catalytic reaction, the observed pH-dependence is likely correlated to steps during the nitrite reduction catalytic cycle. Since the full chemical reaction requires two equivalents of protons, it is not surprising to see that at a lower pH, the reaction rates are higher. Quantitatively, when the pH decreased from 7.0 to 5.8, the proton concentration in the solution [H^+] increased by about 16 times; the rates of the reaction, if directly proportional to [H^+]^2, should have increased by 256 fold. Instead, an increase in rate of ~10-fold is observed for **TRI-H**. The rates for the **TRI-EH** series of peptides similarly increased by about 10–16 fold when the pH changed from 7.0 to 5.8 (Table S4). If one plots Log(Initial rate) = a -b·pH for **TRI-H**, the b co-efficient which corresponds to the proton order of the reaction is 1.25. Thus, while the stoichiometric reaction requires two protons,

the rate-limiting step is dependent on a single proton. The second proton is necessary once the hydroxide leaving group is formed.[24,71,72]

For all the **TRI-EH** peptides, when the pH decreased from 7.4 to 5.8, the reduction potential increased by about 100 mV. If this was the only factor influencing the rates, the NiR reaction rate should have decreased. It is worth noticing that the rates are very low at pH 7.0, so the NiR rates are only analyzed at pH 5.8. As a result, for a specific peptide, when pH decreases from 7.0 to 5.8, the participation of a proton in the rate-limiting step directly enhances the rate, while the significant structural change upon converting from Cu(I) to Cu(II) (reflected as an increased reduction potential) impedes the reaction. This is consistent with the trends observed when comparing the peptides at a fixed proton concentration. Combining these two opposite effects, we observed a 10–16 fold rate increase when the pH decreases from 7.0 to 5.8.

It should be noted that the NiR rate vs. reduction potential correlation at a constant pH should be interpreted with caution as it only compares peptides that contain a Glu in the 22 position. If one compares the parent peptide **TRI-H** and the charge "flipped" peptide **TRI-EH**E27K at pH 5.8 the situation is different. The reduction potential of **TRI-EH**E27K is about 200 mV more positive than that of **TRI-H**, but its NiR rate is only 2 times less than that of the parent peptide. Using the correlation in Figure 9, one would have expected a 6-fold differential between these two peptides if reduction potential *alone* was the determining factor. In general, despite the **TRI-EH** peptides having much more positive reduction potentials, they have, as a group, greater than (or approximately equal) activity compared to **TRI-H**. For example, comparing the rates of Cu(**TRI-H**)$_3$ and Cu(**TRI-EH**)$_3$ at pH 5.8 (Table S4) shows two peptides with similar activities but strongly divergent reduction potentials. This observation points to the importance of Glu at the 22 position for enhancing the rates and suggests the other substitutions made in this series moderate the beneficial impact on catalysis of this Glu22.

Conclusion

We have reported here a systematic approach of modulating the reduction potentials and NiR activities within a self-assembled peptidic framework by stepwise modifications that influence the local charge. These modifications vary the deprotonation equilibria of the Cu(II)-peptides, which have a direct impact on the Cu(II) affinities to the *apo* peptide at different pH conditions. At a specific pH, the influence of the mutations is reflected from the linearly correlated Cu(I)-peptide affinities and Δ_{charge}. Reduction potentials are calculated based on the Cu(I) and Cu(II) affinities to the *apo*-peptides. For a particular peptide, the difference of reduction potentials at different pH conditions originates from the change in Cu(II) affinities; at a specific pH, the difference of reduction potentials for **TRI-EH** series of peptides is dominated by the variance in Cu(I) affinities, which could be the result of the structural perturbation of Cu(I) coordination upon the alteration of charged residues. Moreover, all of these metalloenzymes exhibit pH-dependent NiR activities. For a specific peptide, the NiR rates are governed by the proton concentration and the reduction potentials at different pH conditions. At a specific pH, the reduction potential correlates with the observed rates, however, other factors, such as the formation of substrate-enzyme complex, product-enzyme complex and product release, may also play a role in determining the NiR rates. In particular, the data implicate a key role for a Glu at position 22 in enhancing catalysis. This is likely due to either an H-bond to the His23 or by interaction with the copper-bound substrate.

This study demonstrates that even in highly simplified scaffolds, attempts to change the local charge around the active site may cause multiple interactions that can vary the redox

properties and activities in distinct ways. Nevertheless, this *de novo* design approach allows us to begin to peel the onion layer by layer. Although we still have not drawn a complete picture of the chemistry in this series of peptides, we have demonstrated our ability to isolate different factors (pH, affinities, reduction potentials, *et al*.) and to compare and analyze the effects in a multi-dimensional way. In conclusion, this work showcases the strength of *de novo* protein design to anchor the in-depth understanding of fundamental interactions that modulate the redox properties and NiR activities for a type 2 copper center, which provides interesting insights into future work on model chemistry in general.

Supplementary Material

Refer to Web version on PubMed Central for supplementary material.

Acknowledgments

V. L. P. thanks the National Institutes of Health for financial support of this research (ES012236). F. Y. thanks the Department of Chemistry, University of Michigan for a research fellowship. Portions of this research were carried out at the Stanford Synchrotron Radiation Lightsource, a Directorate of SLAC National Accelerator Laboratory and an Office of Science User Facility operated for the U. S. Department of Energy Office of Science by Stanford University.

References

(1). Prabhulkar S, Tian H, Wang X, Zhu JJ, Li CZ. Antioxid. Redox Signal. 2012; 17:1796–822. [PubMed: 22435347]

(2). Fedurco M. Coord. Chem. Rev. 2000; 209:263–331.

(3). Groves JT. Proc. Natl. Acad. Sci. U.S.A. 2003; 100:3569–3574. [PubMed: 12655056]

(4). Umena Y, Kawakami K, Shen JR, Kamiya N. Nature. 2011; 473:55–60. [PubMed: 21499260]

(5). Castiglione N, Rinaldo S, Giardina G, Stelitano V, Cutruzzolà F. Antioxid. Redox Sign. 2012; 17:684–716.

(6). Klinman JP. Chem. Rev. 1996; 96:2541–2562. [PubMed: 11848836]

(7). Averill BA. Chem. Rev. 1996; 96:2951–2964. [PubMed: 11848847]

(8). Crichton RR, Pierre JL. Biometals. 2001; 14:99–112. [PubMed: 11508852]

(9). Solomon EI, Szilagyi RK, DeBeer George S, Basumallick L. Chem. Rev. 2004; 104:419–58. [PubMed: 14871131]

(10). Rosenzweig AC, Sazinsky MH. Curr. Opin. Struct. Biol. 2006; 16:729–35. [PubMed: 17011183]

(11). MacPherson IS, Murphy MEP. Cell. Mol. Life Sci. 2007; 64:2887–99. [PubMed: 17876515]

(12). Solomon EI, Sundaram UM, Machonkin TE. Chem. Rev. 1996; 96:2563–2606. [PubMed: 11848837]

(13). Solomon EI, Ginsbach JW, Heppner DE, Kieber Emmons MT, Kjaergaard CH, Smeets PJ, Tian L, Woertink JS. Faraday Discuss. 2011; 148:11. [PubMed: 21322475]

(14). Solomon EI, Hadt RG. Coord. Chem. Rev. 2011; 255:774–789.

(15). Solomon EI, Chen P, Metz M, Lee SK, Palmer AE. Angew. Chem., Int. Ed. 2001; 40:4570–4590.

(16). Hannan JP, Busch JLH, Breton J, James R, Thomson AJ, Moore GR, Davy SL. J. Biol. Inorg. Chem. 2000; 5:432–447. [PubMed: 10968614]

(17). Chufán EE, Prigge ST, Siebert X, Eipper B. a, Mains RE, Amzel LM. J. Am. Chem. Soc. 2010; 132:15565–72. [PubMed: 20958070]

(18). Evans JP, Blackburn NJ, Klinman JP. Biochemistry. 2006; 45:15419–29. [PubMed: 17176064]

(19). Kline CD, Mayfield M, Blackburn NJ. Biochemistry. 2013; 52:2586–96. [PubMed: 23530865]

(20). Prigge ST, Eipper B. a, Mains RE, Amzel LM. Science. 2004; 304:864–7. [PubMed: 15131304]

(21). Libby E, Averill BA. Biochem. Biophys. Res. Commun. 1992; 187:1529–1535. [PubMed: 1329738]

(22). Moura I, Moura JJ. Curr. Opin. Chem. Biol. 2001; 5:168–75. [PubMed: 11282344]

(23). Pinho D, Besson S, Brondino CD, de Castro B, Moura I. Eur. J. Biochem. 2004; 271:2361–9. [PubMed: 15182351]

(24). Tocheva EI, Rosell FI, Mauk a G. Murphy MEP. Science. 2004; 304:867–70. [PubMed: 15131305]

(25). Jacobson F, Pistorius A, Farkas D, De Grip W, Hansson O, Sjölin L, Neutze R. J. Biol. Chem. 2007; 282:6347–55. [PubMed: 17148448]

(26). Gray HB, Malmström BG, Williams RJP. J. Biol. Inorg. Chem. 2000; 5:551–559. [PubMed: 11085645]

(27). Saab Rincón G, Valderrama B. Antioxid. Redox Signal. 2009; 11:167–92. [PubMed: 19099403]

(28). Matsuda T, Warshel A. Biochemistry. 1986; 25:1675–1681. [PubMed: 3011070]

(29). Kuila D, Fee JA. J. Biol. Chem. 1986; 261:2768–2771. [PubMed: 3949746]

(30). Varadarajan R, Zewert TE, Gray HB, Boxer SG. Science. 1989; 243:69–72. [PubMed: 2563171]

(31). Hellwig P, Behr J, Ostermeier C, Richter OM, Pfitzner U, Odenwald a, Ludwig B, Michel H, Mäntele W. Biochemistry. 1998; 37:7390–9. [PubMed: 9585553]

(32). Baltzer L, Nilsson H, Nilsson J. Chem. Rev. 2001; 101:3153–63. [PubMed: 11710066]

(33). DeGrado WF, Summa CM, Pavone V, Nastri F, Lombardi A. Annu. Rev. Biochem. 1999; 68:779–819. [PubMed: 10872466]

(34). Bryson JW, Betz SF, Lu HS, Suich DJ, Zhou HX, O'Neil KT, DeGrado WF. Science. 1995; 270:935–41. [PubMed: 7481798]

(35). Ghosh D, Pecoraro VL. Inorg. Chem. 2004; 43:7902–15. [PubMed: 15578824]

(36). Tegoni M, Yu F, Bersellini M, Penner Hahn JE, Pecoraro VL. Proc. Natl. Acad. Sci. U.S.A. 2012; 109:21234–9. [PubMed: 23236170]

(37). Ghadiri MR, Case MA. Angew. Chem., Int. Ed. 1993; 32:1594–1597.

(38). Tanaka T, Mizuno T, Fukui S, Hiroaki H, Oku JI, Kanaori K, Tajima K, Shirakawa M. J. Am. Chem. Soc. 2004; 126:14023–8. [PubMed: 15506765]

(39). Kiyokawa T, Kanaori K, Tajima K, Koike M, Mizuno T, Oku JJII, Tanaka T. J. Pept. Res. 2004; 63:347–53. [PubMed: 15102052]

(40). Hong J, Kharenko O. a, Ogawa MY. Inorg. Chem. 2006; 45:9974–84. [PubMed: 17140193]

(41). Hong J, Kharenko O. a, Fan J, Xie F, Petros AK, Gibney BR, Ogawa MY. Angew. Chem., Int. Ed. 2006; 45:6137–40.

(42). Zastrow ML, Peacock AFA, Stuckey JA, Pecoraro VL. Nat. Chem. 2012; 4:118–123. [PubMed: 22270627]

(43). Chan, WC.; White, PD., editors. Fmoc Solid Phase Peptide Synthesis, A Practical Approach. Vol. Vol. 222. Oxford University Press Inc.; New York: 2000.

(44). Farrer BT, Harris NP, Valchus KE, Pecoraro VL. Biochemistry. 2001; 40:14696–705. [PubMed: 11724584]

(45). Walker, JM., editor. The Protein Protocols Handbook. Second Edi.. Humana Press Inc.; Totowa, NJ: 2002.

(46). Xiao Z, Loughlin F, George GN, Howlett GJ, Wedd AG. J. Am. Chem. Soc. 2004; 126:3081–90. [PubMed: 15012137]

(47). Xiao Z, Wedd AG. Nat Prod Rep. 2010; 27:768–89. [PubMed: 20379570]

(48). Xiao Z, Brose J, Schimo S, Ackland SM, La Fontaine S, Wedd AG. J. Biol. Chem. 2011; 286:11047–55. [PubMed: 21258123]

(49). George, GN. EXAFSPAK. SSRL. Stanford University; USA: 2000. Available at http://ssrl. slac. stanford. edu/exafspak/html. *EXAFSPAK*

(50). Ankudinov A, Rehr J. Physical review B. 1997; 56:R1712–R1716.

(51). Dimakis N, Bunker G. Physical review B. 2002; 65:201103.

(52). Atkins, P.; Overton, T.; Rourke, J.; Weller, M.; Armstrong, F.; Hagerman, M. Inorganic Chemistry. Fifth Edit.. Oxford University Press, W. H. Freeman and Company; New York: 2010.

(53). Kau LS, Spira Solomon DJ, Penner Hahn JE, Hodgson KO, Solomon EI. J. Am. Chem. Soc. 1987; 109:6433–6442.

(54). Perrin BS, Ichiye T. J. Biol. Inorg. Chem. 2013; 18:103–10. [PubMed: 23229112]

(55). Gibney BR, Rabanal F, Reddy KS, Dutton PL. Biochemistry. 1998; 37:4635–43. [PubMed: 9521784]

(56). Shifman JM, Gibney BR, Sharp RE, Dutton PL. Biochemistry. 2000; 39:14813–21. [PubMed: 11101297]

(57). Gibney BR, Isogai Y, Rabanal F, Reddy KS, Grosset a M. Moser CC, Dutton PL. Biochemistry. 2000; 39:11041–9. [PubMed: 10998241]

(58). Gibney BR, Dutton PL. Advances in Inorganic Chemistry. 2001; 68:409–456.

(59). Marshall NM, Garner DK, Wilson TD, Gao YG, Robinson H, Nilges MJ, Lu Y. Nature. 2009; 462:113–6. [PubMed: 19890331]

(60). New SY, Marshall NM, Hor TSA, Xue F, Lu Y. Chem. Commun. (Cambridge, U. K.). 2012; 48:4217–9.

(61). Peacock AFA, Iranzo O, Pecoraro VL. Dalton Trans. 2009; 9226:2271–80. [PubMed: 19290357]

(62). Dieckmann GR, McRorie DK, Lear JD, Sharp KA, DeGrado WF, Pecoraro VL. J. Mol. Biol. 1998; 280:897–912. [PubMed: 9671558]

(63). Sundberg RJ, Martin RB. Chem. Rev. 1974; 74:471–517.

(64). Prenesti E, Daniele PG, Prencipe M, Ostacoli G. Polyhedron. 1999; 18:3233–3241.

(65). Tamilarasan R, Mcmillin DR. Biochem. J. 1989; 263:425–429. [PubMed: 2556993]

(66). Ambundo EA, Deydier M, Grall AJ, Aguera vega N, Dressel LT, Cooper TH, Heeg MJ, Ochrymowycz LA, Rorabacher DB. Inorg. Chem. 1999; 38:4233–4242.

(67). Rorabacher DB. Chem. Rev. 2004; 104:651–97. [PubMed: 14871138]

(68). Bernardo MM, Heeg J, Schroeder IRR, Ochrymowycz LA, Rorabacher DB. Inorg. Chem. 1992; 31:191–198.

(69). Gray HB, Malmström BG. Comments on Inorganic Chemistry. 1983; 2:203–209.

(70). Dong S, Ybe J. a, Hecht MH, Spiro TG. Biochemistry. 1999; 38:3379–85. [PubMed: 10079082]

(71). Antonyuk SV, Strange RW, Sawers G, Eady RR, Hasnain SS. Proc. Natl. Acad. Sci. U.S.A. 2005; 102:12041–12046. [PubMed: 16093314]

(72). Tavares P, Pereira a S. Moura JJG, Moura I. J. Inorg. Biochem. 2006; 100:2087–100. [PubMed: 17070915]

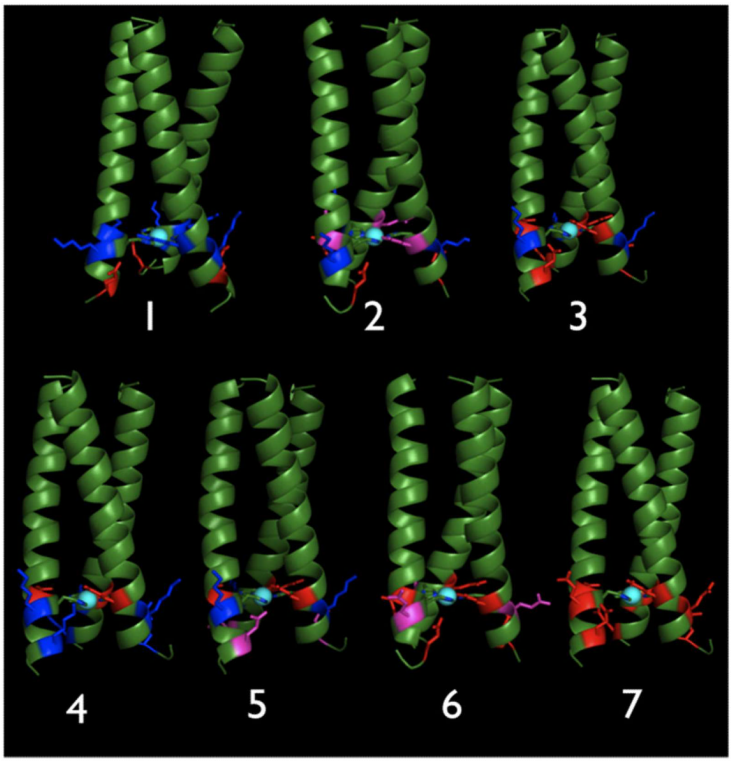

Figure 1.
Pymol models of 1. **TRI-H**, 2. **TRI-H**K22Q, 3. **TRI-EH**, 4. **TRI-EH**E27K, 5. **TRI-EH**E27Q, 6. **TRI-EH**K24Q, 7. **TRI-EH**K24E from the left to the right made based on the crystal structure of $Zn(II)_{-N}Hg(II)_{-S}(CSL9PenL23H)_3$ (PDB code: 3pbj).[42]

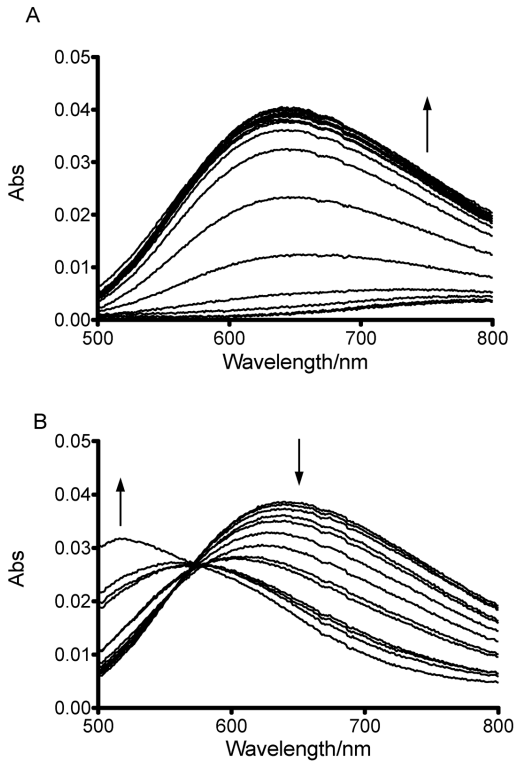

Figure 2.
pH titration spectra of Cu(II)(**TRI-H**)$_3$ at A. lower pH region (pH 2.92–7.45), B. higher pH region (pH 7.60 – 10.80)

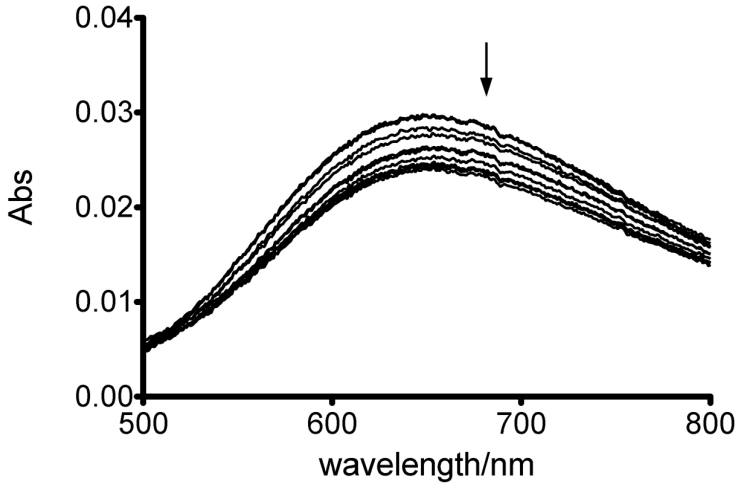

Figure 3.
pH titration spectra of Cu(II)(**TRI-EH**)$_3$ between pH 5.33 and 7.87.

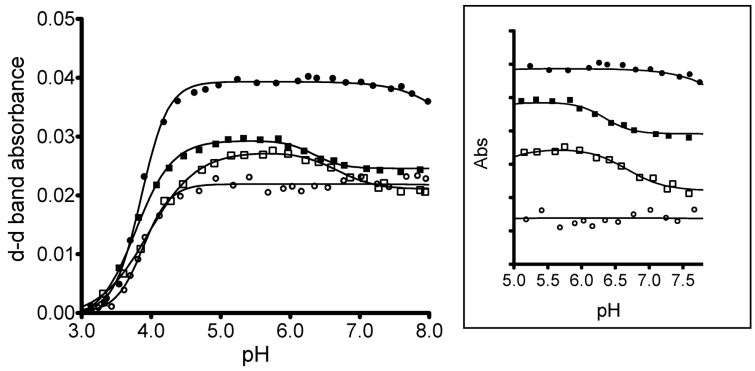

Figure 4.

Changes in Cu(II) d-d band absorbance when bound to **TRI-H** (Δ_{charge} = 0), filled circles; **TRI-EH**E27K (Δ_{charge} = 0), hollow circles; **TRI-EH** (Δ_{charge} = -6), filled squares; and **TRI-EH**K24E (Δ_{charge} = -12), hollow squares; insert: differences between the evolution of Cu(II)-peptide d-d band reveal different pK_a values (same symbols)

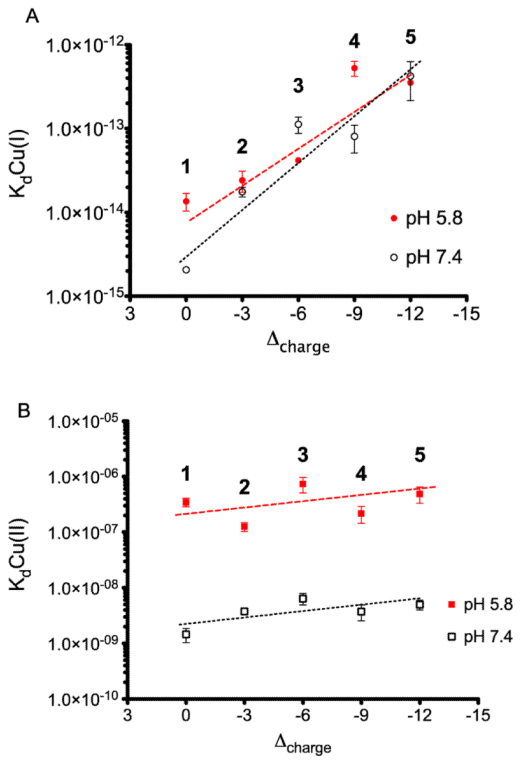

Figure 5.

A. Cu(I) dissociation constants and B. Cu(II) dissociation constants with respect to Δ_{charge} at pH 5.8 and pH 7.4. Peptides: 1) **TRI-EH**E27K; 2) **TRI-EH**E27Q; 3) **TRI-EH**; 4) **TRI-EH**K24Q; 5) **TRI-EH**K24E. Note: the y-axis is on log scales.

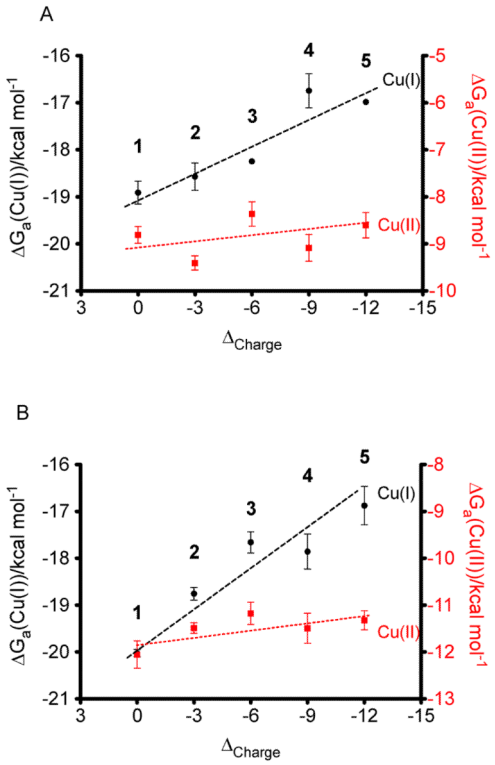

Figure 6.

The free energy of binding for both Cu(I) and Cu(II) at A. pH 5.8; B. pH 7.4. Peptides: 1) **TRI-EH**E27K; 2) **TRI-EH**E27Q; 3) **TRI-EH**; 4) **TRI-EH**K24Q; 5) **TRI-EH**K24E

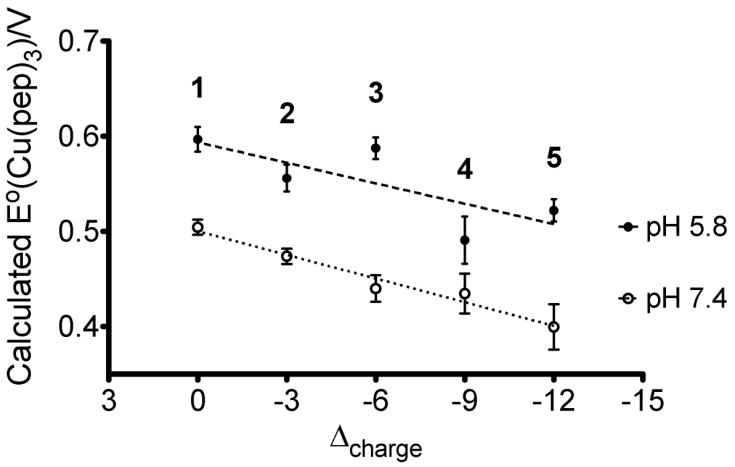

Figure 7.
Calculated reduction potentials in relation to the changes of the local charge at pH 5.8 and 7.4. Peptides: 1) **TRI-EH**E27K; 2) **TRI-EH**E27Q; 3) **TRI-EH**; 4) **TRI-EH**K24Q; 5) **TRI-EH**K24E

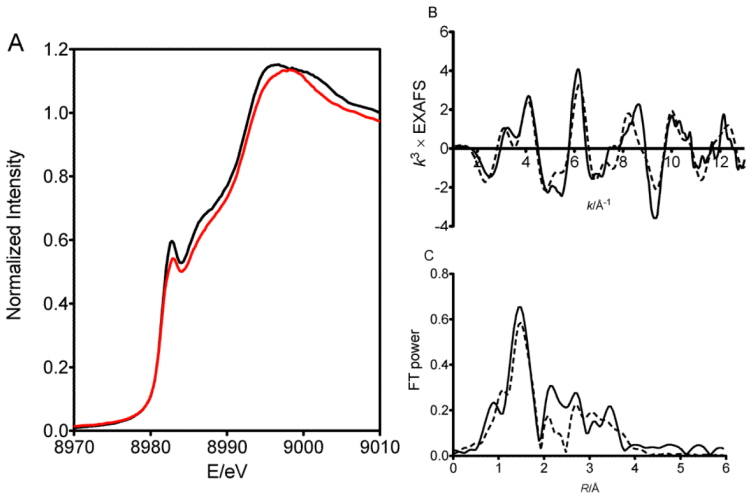

Figure 8.

A. XANES of Cu(I)(**TRI-H**)$_3$ at pH 7.4 (black line) and Cu(I)(**TRI-EH**)$_3$ at pH 8.5 (red line). B. EXAFS of Cu(I)(**TRI-EH**)$_3$ at pH 8.5 (experimental data: solid line; fitting: dashed line). C. Fourier transform of EXAFS in *R* space (experimental data: solid line; fitting: dashed line).

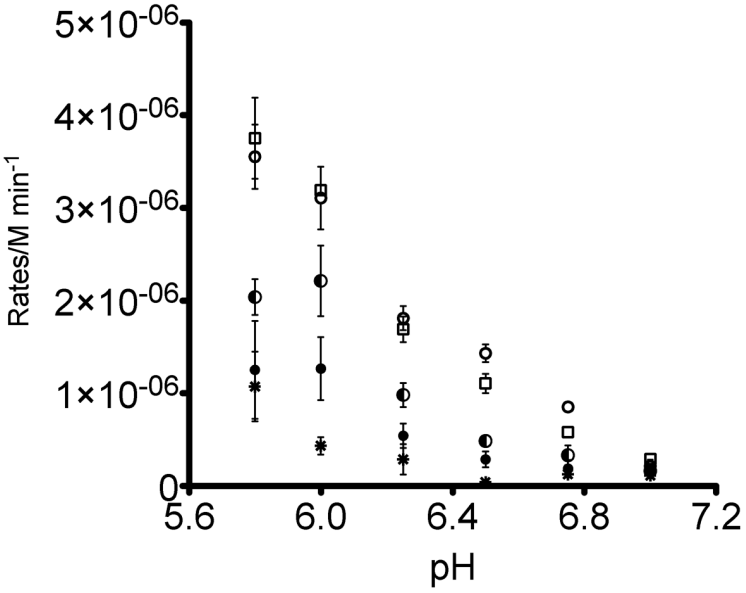

Figure 9.

pH dependece of nitrite reduction rates. Peptides: ○ **TRI-EH**K24E (Δ_{charge} = −12), □ **TRI-EH**K24Q (Δ_{charge} = −9), ◐ **TRI-EH** (Δ_{charge} = −6), ● **TRI-EH**E27Q (Δ_{charge} = −3), ✱ **TRI-EH**E27K (Δ_{charge} = 0).

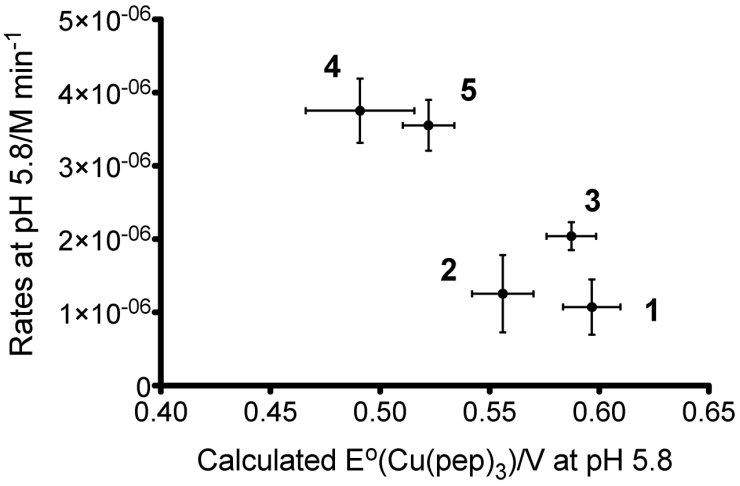

Figure 10.

Rates at pH 5.8 in relation to the calculated reduction potentials at pH 5.8. Peptides: 1) **TRI-EH**E27K; 2) **TRI-EH**E27Q; 3) **TRI-EH**; 4) **TRI-EH**K24Q; 5) **TRI-EH**K24E

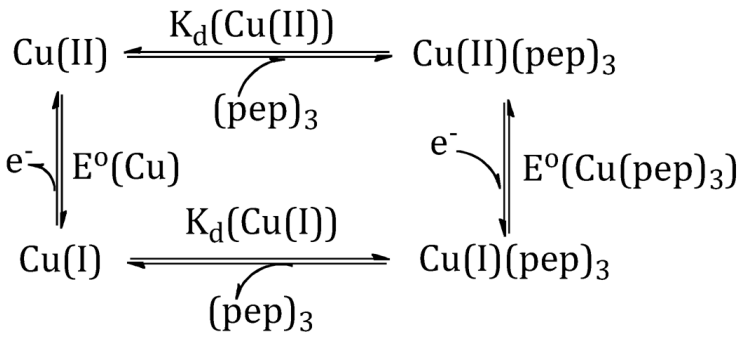

Scheme 1.

Table 1

Peptide sequences used in this study. The color code used throughout corresponds to a change of charge compared to a single **TRI-H** peptide. A difference of −2 charges is given in red, −1 in magenta, +1 in purple and +2 in blue.

Peptide[1]	Sequence	Δ_{charge}[2]
	a b c d e f g a b c d e f g a b c d e f g a b c d e f g	
TRI-H	Ac-G WKALEEK LKALEEK LKALEEK **H**KALEEK G-NH_2	---
TRI-HK22Q	Ac-G WKALEEK LKALEEK LKALEE**Q** **H**KALEEK G-NH_2	-3
TRI-EHE27K	Ac-G WKALEEK LKALEEK LKALEE**E** **H**KAL**K**EK G-NH_2	0
TRI-EHE27Q	Ac-G WKALEEK LKALEEK LKALEE**E** **H**KAL**Q**EK G-NH_2	-3
TRI-EH	Ac-G WKALEEK LKALEEK LKALEE**E** **H**KALEEK G-NH_2	-6
TRI-EHK24Q	Ac-G WKALEEK LKALEEK LKALEE**E** **H****Q**ALEEK G-NH_2	-9
TRI-EHK24E	Ac-G WKALEEK LKALEEK LKALEE**E** **H****E**ALEEK G-NH_2	-12

[1] C-terminus is capped by NH_2 group and N-terminus acetyl (Ac) group.

[2] Δ_{Charge} is defined as the difference in total charge of the specified 3SCC versus (**TRI-H**)$_3$ assuming all Glu are fully deprotonated and all Lys are fully protonated. Polyglutamate or polylysine based ligands can exhibit a wide range of pK_a values when multiple side chains of the same type occur in the same peptide. Therefore, one should recognize that non-integrally charged peptides can exist due to incomplete acid-base chemistry.

Table 2

pK_a values and spectroscopic parameters of selected Cu(II)-peptides

Peptide	pK_a	λ_{max}(ε/M^{-1} cm^{-1})/nm at pH 5.8	λ_{max}(ε/M^{-1} cm^{-1})/nm at pH 7.4
TRI-H	8.53(2)	644(143)	644(143)
TRI-EHE27K	9.59(15)	671(80)	671(79)
TRI-EH	6.33(4)	659(110)	659(89)
TRI-EHK24E	6.76(6)	665(101)	657(81)

Table 3

Cu(I) and Cu(II) dissociation constants at pH 5.8 and pH 7.4

Peptide	Δ_{Charge}	K_d(Cu(I))/M		K_d(Cu(II))/M	
		pH 5.8	pH 7.4	pH 5.8	pH 7.4
TRI-H [36] *	--	$3.09(66) \times 10^{-12}$	$2.00(61) \times 10^{-13}$	$4.04(83) \times 10^{-8}$	$8.69(112) \times 10^{-9}$
TRI-HK22Q	−3	$2.37(27) \times 10^{-14}$	$4.12(114) \times 10^{-14}$	$4.44(59) \times 10^{-7}$	$3.80(106) \times 10^{-9}$
TRI-EHE27K	0	$1.36(56) \times 10^{-14}$	$2.07(27) \times 10^{-15}$	$3.47(104) \times 10^{-7}$	$1.45(71) \times 10^{-9}$
TRI-EHE27Q	−3	$2.42(118) \times 10^{-14}$	$1.76(41) \times 10^{-14}$	$1.26(32) \times 10^{-7}$	$3.76(72) \times 10^{-9}$
TRI-EH	−6	$4.17(19) \times 10^{-14}$	$1.12(43) \times 10^{-13}$	$7.38(324) \times 10^{-7}$	$6.39(258) \times 10^{-9}$
TRI-EHK24Q	−9	$5.38(323) \times 10^{-13}$	$8.06(509) \times 10^{-14}$	$2.18(104) \times 10^{-7}$	$3.73(203) \times 10^{-9}$
TRI-EHK24E	−12	$352(9) \times 10^{-13}$	$4.23(292) \times 10^{-13}$	$4.92\ (225) \times 10^{-7}$	$4.98(173) \times 10^{-9}$

* For **TRI-H**, data were collected at pH 5.9 and 7.4

Table 4

Calculated reduction potentials based on Cu(I) and Cu(II) affinities

Peptide	Δ_{Charge}	E°(Cu-pep$_3$)at pH 5.8/mV	E°(Cu-pep$_3$)at pH 7.4/mV
TRI-H	--	402(8)	433(8)
TRI-HK22Q	−3	589(5)	450(10)
TRI-EHE27K	0	597(13)	504(13)
TRI-EHE27Q	−3	556(14)	474(8)
TRI-EH	−6	587(11)	440(14)
TRI-EHK24Q	−9	491(20)	435(21)
TRI-EHK24E	−12	522(12)	400(20)

For **TRI-H**, calculations were based on affinities at pH 5.9 and 7.4

Table 5

EXAFS fitting parameters[1] of Cu(I)(**TRI-EH**)$_3$

First shell	*R*/Å	σ^2/Å^2	Outer shells	*R*/Å	σ^2/Å^2
3 Cu(I)-N$^{(1)}$	1.93	0.008	3 Cu-C$^{(1)}$	2.91	0.012
			3 Cu-C$^{(2)}$	2.95	0.012
			3 Cu-N$^{(2)}$	4.05	0.010
			3 Cu-C$^{(3)}$	4.06	0.010

The coordination number was held constant at 3 and outer shell parameters were calculated assuming a rigid imidazole ring. Comparison of different models, see Table S6

[1] $\Delta E_0 = -11.94$ eV, R (distance) and σ^2 (Debye-Waller factor) were the only freely variable parameters.

Table 6

EPR parameters of Cu(II)(3SCC)$_3$ at pH 5.8 and 7.4

pH 5.8					
Peptide	$g_\perp$	$g_\parallel$	$A_\perp$/mT	$A_\parallel$/mT	A_{iso}/mT
Cu(II)(**TRI-H**)$_3$	2.05	2.28	0.64	18.58	6.62
Cu(II)(**TRI-EH**E27K)$_3$	2.06	2.27	0.68	17.36	6.24
Cu(II)(**TRI-EH**)$_3$	2.06	2.27	0.36	18.33	6.35
Cu(II)(**TRI-EH**K24E)$_3$	2.06	2.28	0.18	18.33	6.23
pH 7.4					
Peptide	$g_\perp$	$g_\parallel$	$A_\perp$/mT	$A_\parallel$/mT	A_{iso}/mT
Cu(II)(**TRI-H**)$_3$	2.05	2.27	0.64	18.58	6.62
Cu(II)(**TRI-EH**E27K)$_3$	2.05	2.27	1.07	17.50	6.55
Cu(II)(**TRI-EH**)$_3$	2.06	2.27	1.07	18.15	6.76
Cu(II)(**TRI-EH**K24E)$_3$	2.05	2.27	0.71	17.68	6.37